IntelliTorque

ATR

MetaStation 4E

Family of Rheometers

Brabender®

follow us

MORE INFO

SCAN ME

50 East Wesley Street | South Hackensack, NJ. 07606
chemicalsales@cwbrabender.com | 201-343-8425

Effect of Filler Content on the Structure-Property Behavior of Poly(ethylene oxide) Based Polyurethaneurea-Silica Nanocomposites

Oguzhan Oguz,[1,2] Eren Simsek,[1,2] Cagla Kosak Soz,[3] Ozge Kasli Heinz,[1,2] Emel Yilgor,[3] Iskender Yilgor,[3] Yusuf Z. Menceloglu [1,2]

[1]*Faculty of Engineering and Natural Sciences, Materials Science and Nano Engineering, Sabanci University, Orhanli, Tuzla, Istanbul, 34956, Turkey*

[2]*Sabanci University Integrated Manufacturing Technologies Research and Application Center & Composite Technologies Center of Excellence, Teknopark Istanbul, Pendik, Istanbul, 34906, Turkey*

[3]*KUYTAM Surface Science and Technology Center, Chemistry Department, Koc University, Sariyer, Istanbul, 34450, Turkey*

Poly(ethylene oxide) (PEO) based polyurethaneurea-silica nanocomposites were prepared by solution blending and characterized by Fourier Transform Infrared Spectroscopy, Scanning Electron Microscopy, Differential Scanning Calorimetry and tensile testing. The colloidal silica nanoparticles with an average size of 50 nm were synthesized by modified Stöber method in isopropanol. Silica particles were incorporated into three cycloaliphatic polyurethaneurea (PUs) copolymers based on PEO oligomers with molecular weights of 2,000, 4,600, and 8,000 g/mol. Hard segment content of PUs was constant at 30% by weight. Silica content of the PU nanocomposites varied between 1 and 20% by weight. Soft segment (SS) glass transition and melting temperatures slightly increased with increasing filler content for all the copolymers. Degree of SS crystallinity first increased with 1% silica incorporation and subsequently decreased by further silica addition. Elastic modulus and tensile strengths of PU copolymers gradually increased with increasing amount of the silica filler. Elongation at break values gradually decreased in PEO-2000 based PU copolymer with increasing silica content, whereas no significant change was observed in PUs based on PEO-4600 and PEO-8000. Enhancement in tensile properties of the materials was mainly attributed to the homogeneous distribution of silica filler in polymer matrices and strong polymer-filler interactions. POLYM. ENG. SCI., 00:000–000, 2017. © 2017 Society of Plastics Engineers

INTRODUCTION

Polymeric nanocomposites have been a focus of attention particularly because of their enhanced physicochemical, thermal, mechanical, and other engineering properties, enabling their use in a wide range of applications, such as automotive, aerospace, biomedical, sporting goods, and others [1–3]. These complex materials are generally prepared by the incorporation of inorganic fillers into polymer matrices using various processing techniques such as melt-compounding [4], solution blending [5], liquid exfoliation [6], solvent exchange [7], *in situ* polymerization, and so forth [8]. To date, fairy large number of polymeric nanocomposites have been produced using different polymer matrices (amorphous or semicrystalline) and inorganic fillers such as nanoclays [9], nanotubes [10, 11], nanofibers [12, 13], and fumed silica nanospheres [14]. Due to the availability of various polymers and inorganic fillers, the associated functional properties of the nanocomposites can be tailored by modular design approaches [1–8, 15–17] suggesting a high level of control over the structure and morphology. The structure-morphology-property behavior of the nanocomposites mainly depend on the characteristic features of the polymer matrix, the shape, size, that is, aspect ratio, surface area, concentration, and distribution of the filler along with the strength of polymer-filler interactions.

Segmented polyurethane, polyurea, and polyurethaneurea (PUs) copolymers are versatile materials that display interesting combination of composition dependent surface and bulk properties [18–21]. Segmented PU copolymers are mainly formed by the chemical combination of alternating hard and soft segments along a macromolecular backbone. Various soft segments (SS) with glass transition temperatures (T_g) well below room temperature, such as aliphatic polyethers, polyesters, polycarbonates, polyisobutylene, and polydimethylsiloxane and hard segments (HS) consisting of strongly hydrogen bonded urethane and/or urea groups with a T_g or T_m well above the service temperature, can easily be incorporated into PUs [18–21]. Commercial availability of a very large selection of starting materials provides opportunities for the preparation of a wide range of PUs with different chemical compositions. Due to the incompatibility between the HS and SSs, PU copolymers show composition dependent microphase morphologies and interesting combination of bulk and surface properties [18–21]. However, increasing the stiffness and the ultimate strength of PUs while maintaining their extensibility and toughness still present some challenges.

To address this issue, numerous studies have been conducted to investigate the role of different fillers on the mechanical properties of PU based nanocomposites [6, 7, 10, 13, 22–49]. In most of these studies, highly elastomeric PU copolymers with relatively low soft segment molecular weights have been used as polymer matrices for the preparation of nanocomposites using different fillers such as organoclays [7, 31], carbon nanotubes

Correspondence to: I. Yilgor; e-mail: iyilgor@ku.edu.tr or Y.Z. Menceloglu; e-mail: yusufm@sabanciuniv.edu

Contract grant sponsor: Scientific and Technical Research Council of Turkey (TUBITAK); contract grant number: 109M073.

E. Simsek is currently at Quantag Nanotechnologies, Urla, Izmir, Turkey

DOI 10.1002/pen.24672

Published online in Wiley Online Library (wileyonlinelibrary.com).

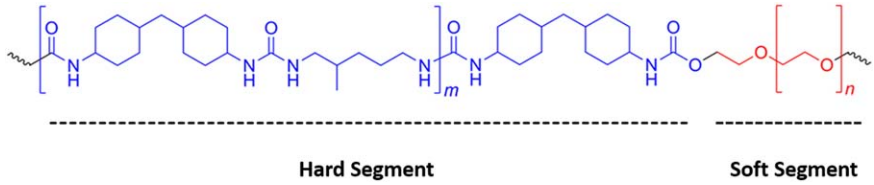

FIG. 1. Chemical structure of PEO based PUs. [Color figure can be viewed at wileyonlinelibrary.com]

[10, 50], halloysite nanotubes [26], cellulose nanocrystals [34, 51], graphene [23, 28], and fumed silica nanoparticles [14]. However, to the best of our knowledge, there is no comprehensive report focusing on the use of polyether based PUs with high SS molecular weights as polymer matrices. Furthermore, limited number of studies has been performed to investigate the effect of colloidal silica nanoparticles on the mechanical behavior of PU nanocomposites. In these studies, silica sol was either added into the polyol solution prior to the reaction with diisocyanate or added into the reaction mixture during the copolymer synthesis to prevent the agglomeration of the nanoparticles [35, 52, 53]. Recently, we reported the use of silica sol "as synthesized and aged" in basic medium for the preparation of PTMO-based PU/silica nanocomposites by solution blending technique [54]. As an extension of this study, here we report the preparation and characterization of PU/silica nanocomposites based on PEO SSs with different molecular weights. Specific focus of this study was the investigation of the effect of PEO molecular weight (2,000, 4,600, and 8,000 g/mol) and silica content on the morphology and properties of the nanocomposites obtained.

EXPERIMENTAL

Materials

PEO glycol oligomers with $<M_n> = 2{,}000$, 4,600, and 8,000 g/mol were purchased from Merck. The chain extender, 2-methyl-1,5- diaminopentane (MDAP) was kindly supplied by DuPont. Bis(4-isocyanatocyclohexyl)methane (HMDI) was kindly provided by Bayer and had a purity better than 99.5%. Dibutyltin dilaurate (DBTDL) was obtained from Witco and is used as a catalyst by diluting to 1 weight % in tetrahydrofuran (THF). Reagent grade 2-propanol (IPA), THF, dimethylformamide (DMF), aqueous ammonia solution (NH_4OH, 25% wt), and tetraethylortosilicate (TEOS, >99%) were obtained from Merck. All chemicals were used as received.

Synthesis of Polyether Based Poly(urethane-urea) Copolymers (PU)

Segmented PUs were synthesized in THF/DMF solution by following the procedure published previously [14, 21, 54]. All reactions were carried out in three-neck, round bottom, Pyrex reaction flasks equipped with an overhead stirrer, a thermometer and an addition funnel, using the two-step prepolymer method. Isocyanate terminated PEO prepolymer was prepared in THF solution with a solids content of 50% by weight, at 60°C using calculated amounts of PEO and HMDI. 150 ppm of DBTDL catalyst in (1% by weight in THF solution) was added and the mixture was stirred at 60°C for 1 h. Progress and completion of the prepolymer reaction was monitored by Fourier Transform Infrared Spectroscopy (FTIR) spectroscopy. After the completion of prepolymer reaction, the solution was cooled down to room temperature and diluted to 25% by weight of solids using DMF. Chain extender (MDAP) was dissolved in DMF (about 10% by weight), introduced into the addition funnel and added dropwise into the reaction mixture until the complete disappearance of the strong isocyanate peak at 2,260 cm^{-1}. The viscosity increase during the chain extension reaction was controlled by adding DMF into the reaction flask. Chemical structure of segmented PU copolymers is shown in Fig. 1. In this figure, the blue and red parts represent the hard and the SSs of PU copolymers, respectively. Various structural characteristics of PU copolymers are summarized in Table 1.

Synthesis of Colloidal Silica Nanoparticles

The colloidal silica nanoparticles were synthesized using the method reported in a previous study [54]. Briefly, the silica sols were prepared in basic medium by modified Stöber method. IPA was used as the alcohol instead of ethanol, which is used conventionally. Sol-gel reactions were performed at room temperature, in 100 mL glass reactors with mixing speeds of 100–300 rpm. IPA and aqueous ammonia were mixed and ultrasonicated for 20 min, and then TEOS was quickly poured into the reactor to initiate the reaction. The sol of colloidal silica nanoparticles was prepared at the molar ratio of $[TEOS]/[NH_3]_{aq} = 1.7$. Hydrodynamic diameter, size distribution of silica nanoparticles in IPA and zeta potential of the silica sol were determined by Dynamic Light Scattering (DLS) analysis performed with Zetasizer Nano (Malvern, UK). Transmission electron microscopy (TEM) analysis was performed using a Philips-FEI Tecnai G2 F20 S-Twin at 200 kV accelerating voltage. A drop of silica sol was deposited on carbon coated Lacey formvar films supported in 300 mesh copper grids (Ted Pella). The grid then was allowed to air-dry for 5 min and oven-dry at 50°C for 15 min.

Preparation of Nanocomposites

The nanocomposites were prepared by dissolving the polyurethane-urea copolymers in THF/DMF (13% solids by weight) and then adding the silica sols into the polymer solutions. The mixtures were stirred on a magnetic stirrer for 96 h, and then, the suspensions were cast into Teflon molds. The solvent was first evaporated at room temperature overnight in a fume hood, followed by drying in an air oven at 60°C for 24 h. Complete removal of the solvents was achieved by drying the films in a vacuum oven at 60°C until constant weight. This was also confirmed by thermogravimetric analyses of the film samples (data not shown in this study). A list of the materials investigated, their compositional details were provided in Table 2. In the sample nomenclature (PU-*X*-*Y*), (*X*) indicated the molecular weight of the PEO used in kilo daltons and (*Y*) the content of colloidal silica nanoparticles by percent weight.

DOI 10.1002/pen

TABLE 1. Structural characteristics of PU copolymers.

Polymer code	$<M_n>$ PEO (g/mol)	$<M_n>$ HS (g/mol)[a]	HS (wt%)	PU $<M_n>$ (g/mol)[b]	PUU $<M_w>$ (g/mol)[b]	DPI (M_w/M_n)
PU-2	2,000	860	30	68,000	100,000	1.48
PU-5	4,600	1,970	30	164,000	232,000	1.42
PU-8	8,000	3,400	30	209,500	309,000	1.47

[a]Calculated from reaction stoichiometry.
[b]Determined by GPC.

Characterization Techniques

FTIR spectra were recorded on a Nicolet 7600 Spectrometer. Solutions were cast on KBr discs and thin films were obtained after evaporating the solvent with an air gun. 32 scans were taken for each spectrum with a resolution of 2 cm^{-1}. ATR-IR spectra were recorded on a Thermoscientific Smart iTR Instrument with Diamond ATR crystal and with an incident angle of 42°. 32 scans were taken for each spectrum with a resolution of 2 cm^{-1}.

Gel Permeation Chromatography (GPC) analyses were performed on a Viscotek GPCmax VE-2001 instrument equipped with D5000-D 3000-D 1000-D Guard columns and RI, LS, DP detectors. DMF was used as the solvent and analysis was performed at 55°C with a flow rate of 1 mL/min. Polymer solutions were prepared in DMF at a concentration of 2 mg/mL. The samples were filtered using VMR PTFE syringe filters with average pore size of 0.45 μm before measurements. Average molecular weights were determined using calibration curves obtained from polystyrene standards. Average molecular weights and molecular weight distributions of the copolymers were listed in Table 1.

A Field-emission-Scanning Electron Microscopy (FE-SEM) (SUPRA 35VP, LEO, Germany) was used to investigate the distribution of silica nanoparticles in composite films. The images were recorded on the cross-sections of the samples fractured in liquid nitrogen and coated with an ultrathin layer of Au/Pd alloy prior to analyses.

Differential Scanning Calorimetry (DSC) analyses were performed on a TA Q2000 instrument calibrated with indium standard and equipped with Tzero functionality that significantly improves the baseline via compensating resistance and capacitance imbalances. All measurements were performed in the range of −160 and 250°C at a heating and cooling rate of 3°C/min under nitrogen atmosphere. The degree of crystallinity (crystalline fraction – X_c) is calculated using the melting enthalpy normalized by the weight fractions of the silica filler and the hard segment, as they do not contribute to the crystallinity of the SS:

$$X_c = \frac{\Delta H_m}{(1-X_f)\times(1-X_{HS})\times\Delta H_{100\%,\ PEO}}\times 100\% \quad (1)$$

where ΔH_m is the melting enthalpy obtained from the area of the melting peak, X_f and X_{HS} are the weight fractions of the silica filler and the hard segment. The melting enthalpy for the 100% crystalline polymer is considered to be equal to that of pure PEO ($\Delta H_{100\%PEO}$), which is reported as 196.8 J/g [55].

Stress-strain analyses were performed on dog-bone type specimens punched out of thin films using a standard die (ASTM D 1708). Measurements were made on a Zwick Z100 model tester under ambient temperature and humidity conditions with a crosshead speed of 25.0 mm/min (L_o= 24.0 mm). At least five specimens were tested for each sample.

TABLE 2. Coding and compositional details of PU/silica nanocomposites investigated.

Coding	HS Content (wt%)	SS Content (wt%)	Silica Content (wt%)
PU-2	30	70	0
PU-2–1	29.7	69.3	1
PU-2–5	28.5	66.5	5
PU-2–10	27	63	10
PU-2–20	24	56	20
PU-5	30	70	0
PU-5–1	29.7	69.3	1
PU-5–5	28.5	66.5	5
PU-5–10	27	63	10
PU-5–20	24	56	20
PU-8	30	70	0
PU-8–1	29.7	69.3	1
PU-8–5	28.5	66.5	5
PU-8–10	27	63	10
PU-8–20	24	56	20

RESULTS AND DISCUSSION

The main aim of this study was the preparation of colloidal silica filled PEO-based segmented PUs with enhanced mechanical properties. To achieve this, the effect of silica filler content on the structure-property behavior of the nanocomposites based on three different segmented PUs with PEO-2000, PEO-4600, and PEO-8000 SSs and a constant hard segment content (30% by weight) was systematically investigated. In particular, the distribution of colloidal silica nanoparticles in polymer matrices was demonstrated by SEM studies on the cross-sectional images of the samples. The polymer-filler interaction was investigated by FTIR spectroscopy. Thermal and mechanical properties of the materials were determined by DSC analyses and tensile tests, respectively. It is important to note that, as shown in Table 1, as the hard segment content in PUs is constant, as the molecular weight of PEO increases so does the molecular weight of the urea hard segments. Increased urea hard segment length, which improves the microphase separation in PU also influences the interaction of the matrix with silica nanoparticles.

Preparation and Characterization of Colloidal Silica Nanoparticles

Results obtained from TEM and DLS analyses of the colloidal silica nanoparticles are presented in Fig. 2. Figure 2a provides the TEM image of uniform, spherical silica particles obtained with an average diameter of 50 ± 7.2 nm. In addition, Fig. 2b displays the intensity distribution of hydrodynamic diameter of colloidal silica nanoparticles in IPA. As shown in Fig. 2b, the average hydrodynamic diameter of SiO_2

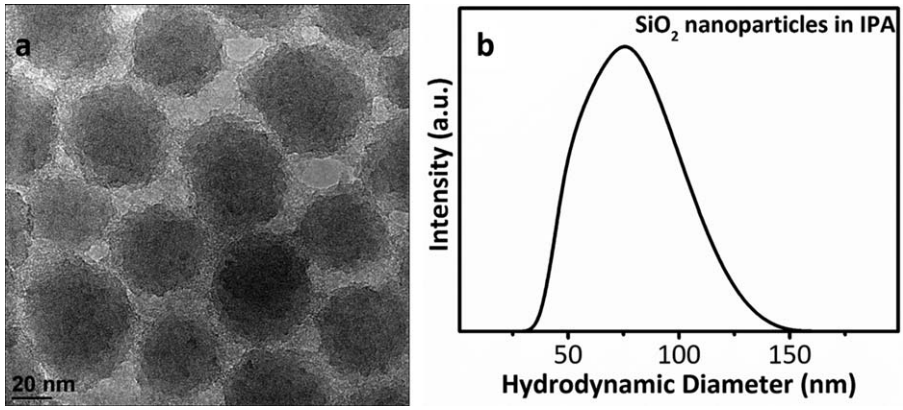

FIG. 2. (a) TEM image of the colloidal silica nanoparticles. (b) Hydrodynamic diameter of colloidal silica nanoparticles in IPA.

nanoparticles in IPA is recorded as 74 ± 0.2 nm with a polydispersity index value of 0.1 ± 0.03, and a zeta potential of -74 ± 7.1 mV as in accordance with the results reported in an earlier study [54].

SEM Studies

To achieve optimum properties, homogeneous distribution of nanoparticles in polymer matrices is critical. SEM is a simple and quantitative method for the investigation of the nature of silica nanoparticle distribution in PU copolymer matrices. Cross-sectional SEM images of different polyurethanes containing 20% by weight silica, PU-2–20, PU-5–20, and PU-8–20 are shown in Fig. 3. As can be seen in the SEM micrographs provided, all nanocomposites display quite homogeneous silica distribution regardless of the molecular weight of the PEO SSs. These results indicate good interaction between polar PU matrix and hydrophilic silica particles. Interactions can be between the hydroxyl groups present on silica particles and the ether groups of PEO SSs or urethaneurea hard segments, through hydrogen bonding and/or dipole–dipole interaction. To clarify the nature and the extent of interactions between the PU matrix and silica particles, FTIR spectroscopy was used.

FTIR Spectroscopy Studies

FTIR spectroscopy is a simple and useful technique for the investigation of the hydrogen bonding interactions in polyurethanes, where it is possible to get qualitative and quantitative information [56]. Figure 4 displays the full-scale FTIR spectra of PU-2, PU-5, PU-8 copolymers and silica nanoparticles. For

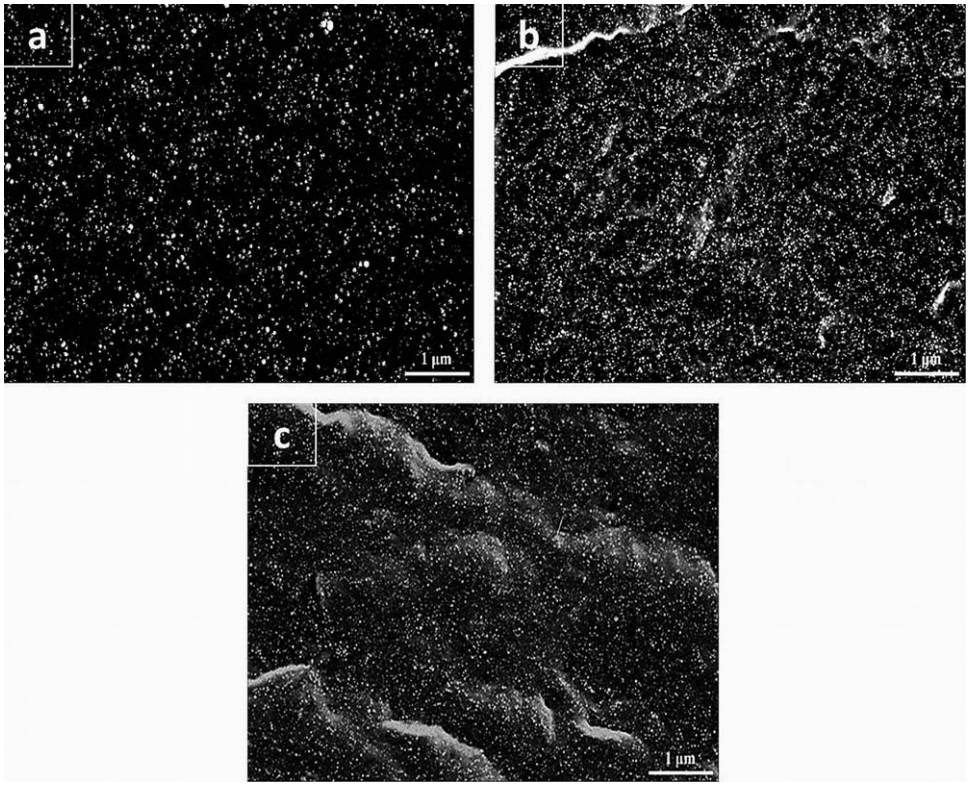

FIG. 3. Cross-sectional SEM images of (a) PU-2–20, (b) PU-5–20, and (c) PU-8–20.

DOI 10.1002/pen

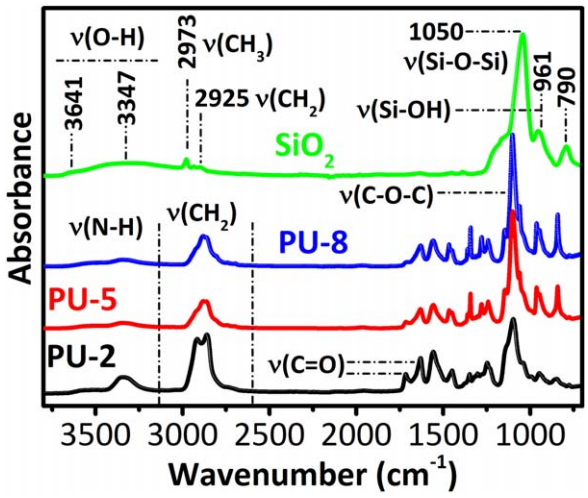

FIG. 4. FTIR spectra of PU-2 (black), PU-5 (red), and PU-8 (blue) copolymers and SiO_2 nanoparticles (green). [Color figure can be viewed at wileyonlinelibrary.com]

copolymers, typical N—H (3,600–3,000 cm^{-1}), CH_2 (3,000–2,600 cm^{-1}), C═O (1,800–1,600 cm^{-1}), and C—O—C (1,110–1,090 cm^{-1}) stretching vibrations are shown in Fig. 4 [56]. Along with this, the absorption bands arising from O—H (3,600–3,000 cm^{-1}), CH_3 (2973 cm^{-1}), CH_2 (2925 cm^{-1}), Si—O—Si (1,050 and 790 cm^{-1}) and Si—OH (961 cm^{-1}) stretching vibrations are presented in the FTIR spectrum of silica nanoparticles given in Fig. 4 [57]. The O—H stretching vibrations are basically arisen from the H-bonded Si-OH groups in the nanocomposites. The absorption bands at 1,050 and 790 cm^{-1} mainly represent the asymmetric and symmetric vibrations of Si—O—Si, respectively [57]. The peaks at 2,973 and 2,925 cm^{-1} can be used to probe the presence of unreacted TEOS in the SiO_2 nanoparticles [57].

In the PU-silica nanocomposites investigated, major type of interactions between silica nanoparticles and PEO based PU matrix are expected to be through hydrogen bonding of surface hydroxyl groups in silica with the ether (C—O—C) groups in PEO SSs and the urea groups in the hard segments. Therefore, we mainly focused on 1,200–1,000 cm^{-1} region to study the silica/ether interactions and 1,800–1,600 cm^{-1} region to investigate the silica/urea interactions as a function of silica concentration in the nanocomposites. Ether region of the FTIR spectra of PU-2 and nanocomposites containing 1, 5, 10, and 20% by weight silica are reproduced in Fig. 5a. As shown in Fig. 5a, ether group in PU-2 displays a strong absorption peak centered at 1,091 cm^{-1} due to (C—O—C) stretching. On the addition of silica nanoparticles this peak shifts to lower wavenumbers and shows some broadening. We believe this shift is due to the interaction of hydroxyl groups on silica nanoparticles with the ether oxygen of the PEO SSs via hydrogen bonding. The peak broadening is probably due to the overlapping of the C-O-C bands in PEO, with that of the Si—O—Si stretching of the silica nanoparticles, which shows a strong doublet at 1,093–1,024 cm^{-1}.

Carbonyl region of the FTIR spectra for PU-2 and nanocomposites are provided in Fig. 5b. Urethaneurea hard segments in PU-2 display two well defined peaks centered at 1,715 and 1,632 cm^{-1}, due to weakly and strongly hydrogen bonded (C═O) absorptions, from urethane and urea groups, respectively [56]. There is no notable change in the position or shape of the urethane carbonyl peak at 1,715 cm^{-1} by the increasing amount of the silica filler. Conversely, a clear shift in the urea carbonyl peak at 1,632–1,648 cm^{-1} is observed with the addition of 20% by weight silica nanoparticles. These results indicate that silica nanoparticles preferentially interact with strongly hydrogen bonded urea groups in nanocomposites as compared to urethanes. This may be expected, as the concentration of urea groups in PU-2 is much higher than urethanes. Fairly similar behavior is observed in the FTIR investigation of PU/silica nanocomposites based on PU-5 and PU-8. Ether and carbonyl regions of the FTIR spectra for these systems as a function of silica concentration are provided in Figs. 6 and 7, respectively. As shown in Fig. 6a, the shifts in the ether peak of PU-5/silica nanocomposites with high silica contents are very similar to that of PU-2 series. Conversely, no significant shift is observed for the nanocomposites with 1 and 5 wt% silica nanoparticles. Very similar behavior is also observed in ether stretching peaks of PU-8 based silica nanocomposites as shown in Fig. 7a. As will be discussed in the next section, we believe this is due to highly crystalline nature of the PU-5 and PU-8 matrices, when compared to PU-2. As shown in Figs. 6b and 7b, no significant change in the urethane (1,725 cm^{-1}) and urea (1,632 cm^{-1}) carbonyl peak positions are observed in silica nanocomposites based on PU-5 and PU-8 indicating fairly weak interaction of silica with the hard segments.

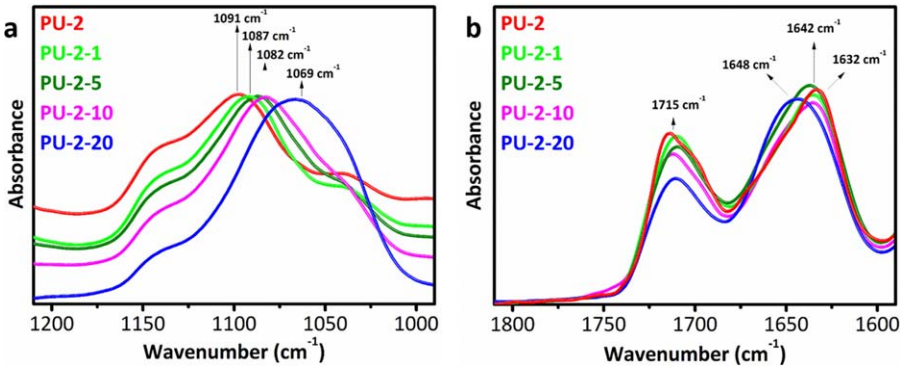

FIG. 5. FTIR spectra of (a) ether (C—O—C) stretching absorption peaks and (b) carbonyl (C═O) region in PU-2 and PU-2/silica nanocomposites as a function of silica content. [Color figure can be viewed at wileyonlinelibrary.com]

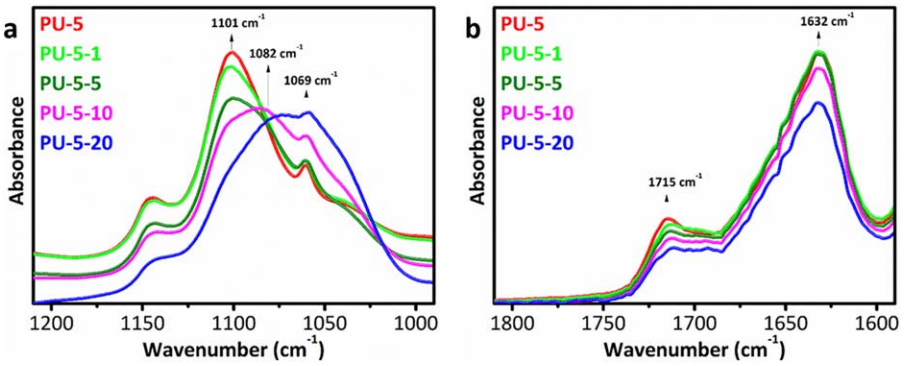

FIG. 6. FTIR spectra of (a) ether and (b) carbonyl regions of PU-5 and PU-5/silica nanocomposites as a function of the silica content. [Color figure can be viewed at wileyonlinelibrary.com]

Thermal Properties by DSC

Segmented polyurethanes and PUs display microphase separation, which is strongly dependent on their composition, structure and molecular weight of the SSs [21]. In PEO based PUs, depending on their molecular weight and amount in the copolymer, PEO matrix displays crystallinity. DSC thermograms of PU copolymers and PU/silica nanocomposites are reproduced in Fig. 8. The results obtained from the thermal analyses of the samples are listed in Table 3. As can be seen in Fig. 8a and Table 3, PU-2 and PU-2/silica nanocomposites all display well defined glass transitions in −58°C to −52°C range, followed by a small crystallization exotherm between −50 and −25°C and a sharp melting at 20°C–25°C. PU-5 (Fig. 8b) and PU-8 (Fig. 8c) copolymers, which are highly crystalline when compared to PU-2, show very weak glass transition temperatures in −52°C to −44°C range followed by sharp melting endotherms, as summarized in Table 3. To provide a clear overview on T_g values of PU-5 and PU-8 based samples, the glass transition regions of corresponding DSC thermograms are reproduced in Fig. 9. As listed in Table 3, PEO SS T_g values are determined as −57.2, −51.9, and −48.9°C for PU-2, PU-5, and PU-8 copolymers, respectively. This is expected, as T_g values of PEO oligomers are reported to increase with molecular weight [58]. As shown in Fig. 8d, in all nanocomposites, T_g values of the PEO matrix increase linearly as a function of the silica content. These results strongly support the observations made in FTIR studies, which suggested stronger interaction between PEO matrix and silica, when compared with silica and hard segments.

Melting temperatures (T_m) and degree of crystallinity of PEO SSs (X_c), which is calculated using *Eq. 1* given above, are also listed in Table 3 for all the copolymers and their nanocomposites. In all nanocomposites, the degree of crystallinity of PEO SS slightly increased by the addition of 1 wt% of silica, which might have acted as a nucleating agent, and then subsequently decreased by the further addition of silica nanoparticles.

As can be seen in Table 3, in all nanocomposites, a decreasing trend in the ΔC_p values at T_g is observed. The magnitude of the decrease is higher in PU-2 based systems when compared with those of PU-5 and PU-8. This is mainly due higher crystallinity of PEO matrices in PU-5 and PU-8 when compared with PU-2 as can be seen in Table 3. The decreasing trend in the ΔC_p at T_g in the nanocomposites shows the restriction imposed on the chain movements due to strong interaction between the PEO matrix and silica filler.

DSC results mainly suggest that the thermal properties of the copolymers can be tuned by the addition of silica nanoparticles. However, to evaluate and compare the tensile properties of these materials properly, it must be noted that the melting points of PU-2 and all of its nanocomposites are below room temperature, indicating a mainly amorphous PEO matrix. In contrast, PU-5, PU-8 and their nanocomposites have crystalline PEO matrices.

Tensile Properties

Stress-strain curves for all materials are provided in Figs. 10–12, where expanded initial regions (0–100% elongation) are also given. Young's modulus (E), ultimate tensile strength

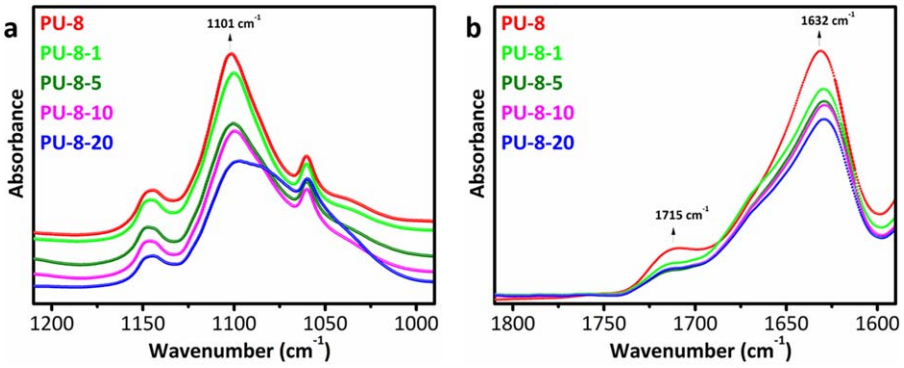

FIG. 7. FTIR spectra of (a) ether and (b) carbonyl regions of PU-8 and PU-8/silica nanocomposites as a function of the silica content. [Color figure can be viewed at wileyonlinelibrary.com]

DOI 10.1002/pen

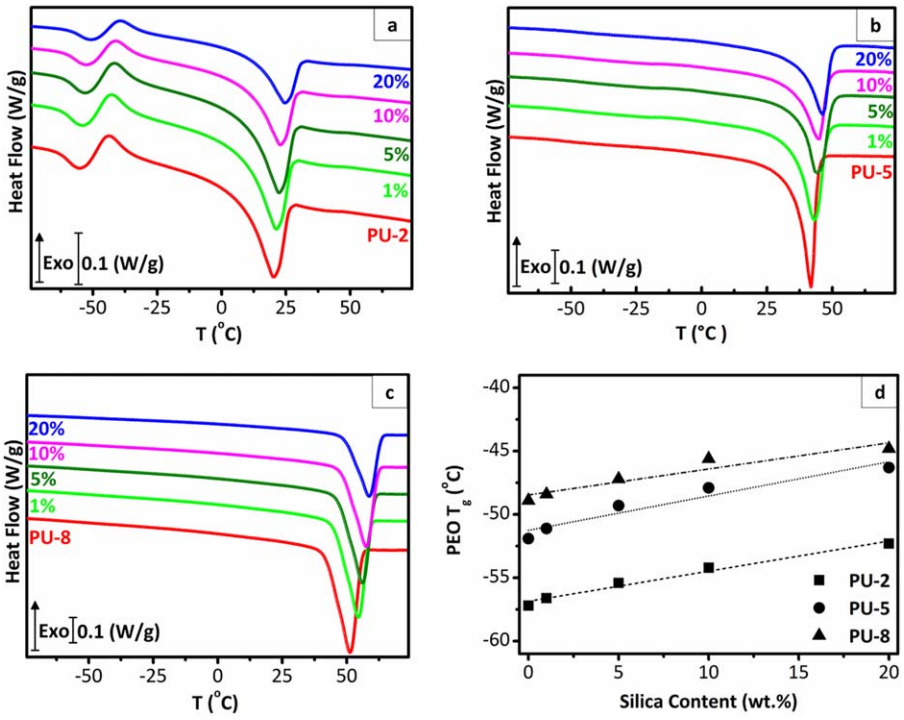

FIG. 8. DSC thermograms of (a) PU-2, (b) PU-5, (c) PU-8 based nanocomposites, and (d) variation of PEO matrix T_g as a function of silica content. [Color figure can be viewed at wileyonlinelibrary.com]

(σ_{max}), percent elongation at break (ε), and tensile toughness (W) (work to fracture) values obtained from stress-strain measurements for all the nanocomposites and PUs are provided in Table 4. Figures 10–12 clearly demonstrate that in all PU/silica nanocomposites, ultimate tensile strengths increase dramatically from about 30 MPa to around 50 MPa, with the silica content. The strengthening of PU copolymers was mainly attributed to the strong physical interactions between the PEO matrix and silica filler through hydrogen bonding. Interestingly, in PU-2 based nanocomposites (Fig. 10), elongation at break decreases gradually from 1,000% for PU-2 to about 650% for PU-2–20. No significant decrease in elongation at break is observed for PU-5 and PU-8 based nanocomposites (Figs. 11 and 12). PU-2 based samples show typical elongation behavior of amorphous polyether based elastomeric PU/silica nanocomposites reported in a previous study [54]. On the contrary, PU-5 and PU-8 samples display typical behavior of highly crystalline thermoplastic PU elastomers.

As expected, and as can be seen in Table 4, Young's modulus values also increase with increasing silica content in all nanocomposites. The increases in modulus basically arisen from the difference between the elastic constants of the polymer and the filler as suggested by the composite theory. Expectedly, the mechanically restrained polymer chains around the nanoparticles

TABLE 3. Thermal properties and degree of crystallinity values of PEO segments in PEO based PU/silica nanocomposites determined from DSC thermograms.

Sample	T_g (°C)	ΔC_p at T_g (J/g K)	T_m (°C)	$^{DSC}\Delta H_m$ (J/g)	$^{normalized}\Delta H_m$ (J/g)	X_c (%)
PU-2	−57.2	0.485	19.9	44.9	64.1	32.6
PU-2–1	−56.6	0.334	21.2	45.3	65.1	33.1
PU-2–5	−55.4	0.249	22.3	43.2	63.5	32.3
PU-2–10	−54.2	0.167	23.6	37.1	56.4	28.7
PU-2–20	−52.3	0.142	24.8	24.9	40.9	20.8
PU-5	−51.9	0.113	42.1	59.9	85.5	43.5
PU-5–1	−51.1	0.097	43.2	60.5	86.9	44.2
PU-5–5	−49.3	0.086	43.6	57.6	84.7	43.1
PU-5–10	−47.9	0.081	44.9	49.5	75.3	38.3
PU-5–20	−46.3	0.067	46.3	32.6	53.5	27.2
PU-8	−48.9	0.058	51.2	77.6	110.9	56.4
PU-8–1	−48.4	0.049	54.3	78.2	112.3	57.1
PU-8–5	−47.2	0.038	56.2	74.6	109.7	55.8
PU-8–10	−45.6	0.022	57.3	67.1	102.1	51.9
PU-8–20	−44.8	0.011	58.4	51.1	84.0	42.7

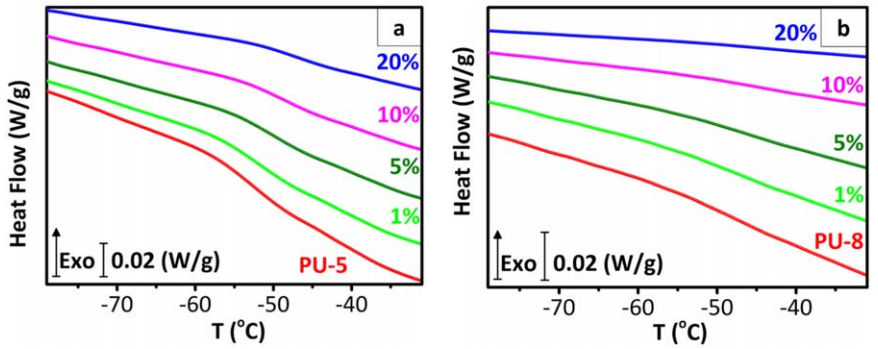

FIG. 9. The glass transition region in DSC thermograms of (a) PU-5 and (b) PU-8 copolymers and their nanocomposites reinforced by silica nanoparticles. [Color figure can be viewed at wileyonlinelibrary.com]

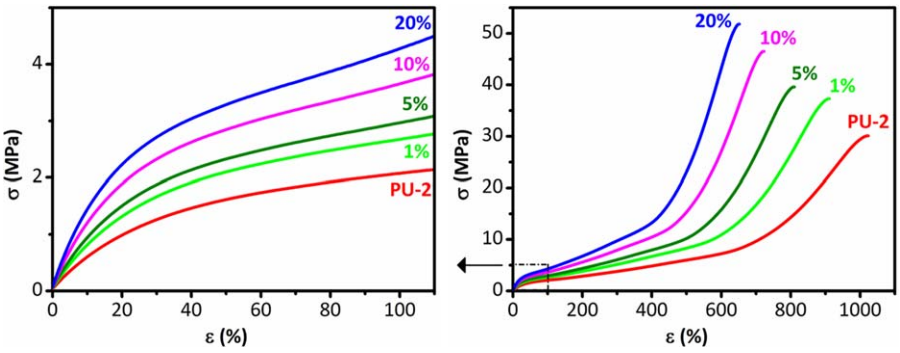

FIG. 10. Expanded initial region (left) and complete stress-strain curves (right) of PU-2 and PU-2/silica nanocomposites. [Color figure can be viewed at wileyonlinelibrary.com]

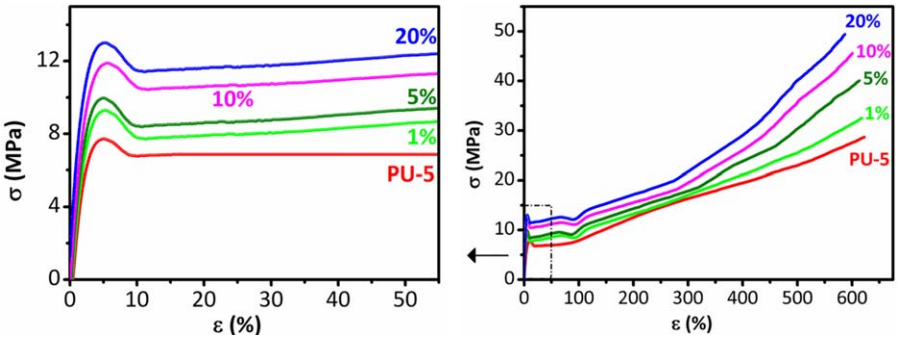

FIG. 11. Expanded initial region (left) and complete stress-strain curves (right) of PU-5 and PU-5/silica nanocomposites. [Color figure can be viewed at wileyonlinelibrary.com]

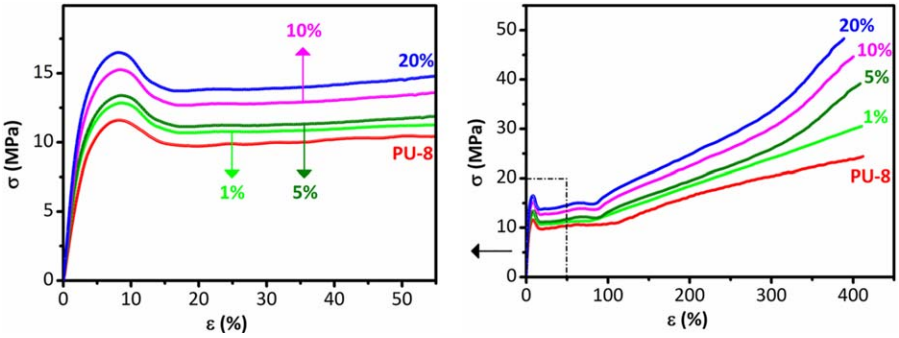

FIG. 12. Expanded initial region (left) and complete stress-strain curves (right) of PU-8 and PU-8/silica nanocomposites. [Color figure can be viewed at wileyonlinelibrary.com]

DOI 10.1002/pen

TABLE 4. Summary of tensile properties of PEO based PU/silica nanocomposites.

Sample	(E) (MPa)	$\%\Delta E$	(σ_{max}) (MPa)	$\%\Delta\sigma_{max}$	ε (%)	%Δε	W (MJm^{-3})	$\%\Delta W$
PU-2	5.1 ± 0.3	Ref	30.1 ± 1.1	Ref	1000 ± 65	Ref	94 ± 7	Ref
PU-2–1	7.3 ± 0.1	+43.1	37.3 ± 1.3	+23.9	910 ± 40	−9.0	104 ± 3	+10.7
PU-2–5	8.4 ± 0.8	+64.7	39.6 ± 1.1	+31.5	810 ± 30	−19.0	103 ± 3	+10.0
PU-2–10	12.9 ± 0.6	+152.9	46.5 ± 1.2	+54.4	720 ± 20	−28.0	104 ± 3	+10.3
PU-2–20	29.6 ± 4.0	+480.3	51.8 ± 1.6	+72.1	650 ± 10	−35.0	103 ± 3	+10.0
PU-5	145 ± 19	Ref	28.7 ± 1.3	Ref	630 ± 50	Ref	103 ± 8	Ref
PU-5–1	193 ± 8	+33.0	32.8 ± 1.4	+14.3	620 ± 20	−1.3	113 ± 4	+9.5
PU-5–5	225 ± 13	+54.2	39.7 ± 1.7	+38.3	615 ± 20	−2.1	122 ± 4	+18.8
PU-5–10	320 ± 18	+120.2	45.6 ± 2.1	+58.9	600 ± 10	−4.3	136 ± 3	+31.8
PU-5–20	520 ± 16	+261.0	49.5 ± 1.9	+72.4	590 ± 30	−6.4	145 ± 4	+40.5
PU-8	370 ± 20	Ref	24.4 ± 3.4	Ref	410 ± 35	Ref	67 ± 6	Ref
PU-8–1	455 ± 23	+23.1	30.5 ± 2.3	+25.0	410 ± 10	−1.0	78 ± 3	+16.1
PU-8–5	530 ± 20	+44.0	39.2 ± 2.1	+60.6	405 ± 20	−2.2	86 ± 4	+27.4
PU-8–10	665 ± 24	+80.1	44.6 ± 2.4	+82.8	400 ± 30	−2.9	96 ± 4	+42.3
PU-8–20	875 ± 15	+136.0	48.3 ± 1.6	+97.9	390 ± 40	−5.6	100 ± 5	+49.3

allow for a considerable amount of the load to be transferred to the silica [24, 59]. Since the nanoparticles are homogeneously distributed in the polymer matrices, the portion of restrained polymer is gradually increased by increasing filler content giving rise to an increase in the elastic modulus. In addition, as listed in Table 4, it is interesting to note that the percent increase in the modulus ($\%\Delta E$) as a function of filler content is higher for PU-2 as compared to that of PU-5, which is also higher than that of PU-8. For instance, $\%\Delta E$ is around fivefold (480%) for PU-2–20 in comparison to that of PU-2, whereas $\%\Delta E$ values are around 2.5-fold (261%) for PU-5–20, and 1.3-fold (136%) for PU-8–20 as compared to those of PU-5 and PU-8, respectively. It is likely that the stiffening effect of silica nanoparticles is inversely proportional to the degree of crystallinity of PEO matrix. As a plausible explanation, this might be due to the following reason: The increase in PEO SS molecular weight results in an increase in the degree of crystallinity of soft block, that is, the matrix phase, in PU copolymers. The increase in the degree of crystallinity of the PEO matrix mainly corresponds to a decrease in its amorphous fraction. The decrease in the amorphous portion of the PEO matrix basically indicates a decrease in the number of available sites (ether oxygen), which can directly interact with the hydroxyl groups on the silica surfaces via hydrogen bonding. This decrease affects the interfacial stress transfer between the matrix and the filler, and eventually leads to relatively less effective stiffening.

Conversely, another interesting but expected observation based on the DSC results, is the necking or yielding displayed by the PU-5 and PU-8 based nanocomposites with crystalline PEO SSs (Figs. 11 and 12), when compared with amorphous PU-2 based systems, which do not show necking (Fig. 10).

It is well known that the area under a stress-strain curve directly represents the energy per unit volume required for failure of the sample and thus provides a quantitative value of the toughness. A slight increase (about 10%) in the tensile toughness of PU-2 was observed by the incorporation of 1% by weight silica. However, no significant increase was observed by further addition of silica nanoparticles, due to significant reduction in elongation at break, which strongly affected the area under the stress-strain curve. On the contrary, PU-5 and PU-8 based nanocomposites displayed gradual increase in the tensile toughness with an increase in the amount of silica filler. The toughness of PU-5 increased from 103 ± 7.8 MJm^{-3} to 144.7 ± 4.4 MJm^{-3}, whereas that of PU-8 went up from 67.2 ± 5.7 MJm^{-3} to 100.3 ± 5.2 MJm^{-3} on the incorporation of 20% by weight of silica nanoparticles. Similar results were also observed for PDMS based PU/silica nanocomposites as previously reported by our group [14].

Recently, Gersappe suggested that the mobility of nanoparticles in a polymer matrix plays a key role in the toughening of nanocomposites. This mobility is defined as a complex function of the filler size, the attraction between the polymeric matrix and filler and the thermodynamic state of the matrix [60]. Basically, the ability of the nanoparticles to enhance the materials toughness originates from the equivalent time scales of motion for the polymer and filler. This hypothesis was evidenced by Giannelis and his coworkers in a study focused on treated nanoclay reinforced poly(vinylidene fluoride) based nanocomposites [61]. They mainly suggested that the addition of nanoclays provides significant toughening effect to the nanocomposites when the tensile tests were performed at a temperature higher than the glass transition temperature of the polymer [61]. Most recently, Zhou and co-workers investigated the nanoparticle mobility in nanosized silica reinforced thermoplastics as an example of nonlayered polymeric nanocomposites [62]. They mainly suggested that in addition to the mobility of the polymeric matrix, the mobility of the nanofiller was critical in improving the toughness of the nanocomposite. To achieve this, good polymer-filler interaction but minimum particle–particle interaction was required [62]. Since all these preconditions were evidenced by DSC, FTIR, and SEM studies for our samples, we believe that the mobility of colloidal silica nanoparticles in PU matrices is a key parameter for the enhanced material toughness demonstrated by the stress-strain analyses. In addition, our results suggest that this mechanism is much more effective to toughen the PU copolymers with highly crystalline SSs as demonstrated in PU-5 and PU-8 based nanocomposites.

CONCLUSIONS

Three different poly(ethylene oxide) (PEO) based poly(urethane-urea) (PU) copolymers with constant hard segment content of 30% by weight and colloidal silica nanoparticles with average diameters of 50 nm were used for the preparation of PU/silica

nanocomposites. The nanocomposites containing 1, 5, 10, and 20% by weight silica were prepared by solution blending. The effect of PEO molecular weight in PU ($<M_n> = 2{,}000$, 4,600, and 8,000 g/mol) and the amount of the silica filler on the structure-property behavior of nanocomposites was systematically investigated by FTIR, SEM, DSC, and stress-strain tests. Strong polymer-filler interaction and quite homogeneous distribution of silica nanoparticles in polymer matrices were evidenced by FTIR and SEM studies, respectively. Glass transition temperatures (T_g) of SS matrix increased and ΔC_p values at T_g decreased as a function of the silica content in all nanocomposites regardless of the PEO molecular weight. Melting temperatures of the PEO matrix also increased by increasing amount of silica nanoparticles. The degree of SS crystallinity, first, increased with 1% silica addition and then decreased for all the nanocomposites investigated.

The elastic modulus and tensile strength values of the PU copolymers gradually increased by increasing amount of the silica filler. Furthermore, the elongation at break values gradually decreased with increasing silica content in nanocomposites prepared from PU copolymer based on PEO-2000 SSs (PU-2), whereas no notable change was observed in the PEO-4600 (PU-5) and PEO-8000 (PU-8) based nanocomposites. This resulted in relatively small improvement in the tensile toughness (about 10%) of PU-2 based silica nanocomposites, while for PU-5 and PU-8 based nanocomposites with 20% silica toughness values improved significantly by 40% and 50%, respectively, when compared with the parent PU matrices.

REFERENCES

1. J. Jancar, J. F. Douglas, F. W. Starr, S. K. Kumar, P. Cassagnau, A. J. Lesser, S. S. Sternstein, and M. J. Buehler, *Polymer*, **51**, 3321 (2010).
2. D. W. Schaefer and R. S. Justice, *Macromolecules*, **40**, 8501 (2007).
3. H. Zou, S. Wu, and J. Shen, *Chem. Rev.*, **108**, 3893 (2008).
4. C. H. Dan, M. H. Lee, Y. D. Kim, B. H. Min, and J. H. Kim, *Polymer*, **47**, 6718 (2006).
5. W. Zha, C. D. Han, H. C. Moon, S. H. Han, D. H. Lee, and J. K. Kim, *Polymer*, **51**, 936 (2010).
6. J. N. Coleman, M. Lotya, A. O'Neill, S. D. Bergin, P. J. King, U. Khan, K. Young, A. Gaucher, S. De, R. J. Smith, I. V. Shvets, S. K. Arora, G. Stanton, H.-Y. Kim, K. Lee, G. T. Kim, G. S. Duesberg, T. Hallam, J. J. Boland, J. J. Wang, J. F. Donegan, J. C. Grunlan, G. Moriarty, A. Shmeliov, R. J. Nicholls, J. M. Perkins, E. M. Grieveson, K. Theuwissen, D. W. McComb, P. D. Nellist, and V. Nicolosi, *Science*, **331**, 568 (2011).
7. S. M. Liff, N. Kumar, and G. H. McKinley, *Nat. Mater.*, **6**, 76 (2007).
8. K. Saeed, S.-Y. Park, H.-J. Lee, J.-B. Baek, and W.-S. Huh, *Polymer*, **47**, 8019 (2006).
9. S. Sinha Ray, and M. Okamoto, *Prog. Polym. Sci.*, **28**, 1539 (2003).
10. H. Koerner, G. Price, N. A. Pearce, M. Alexander, and R. A. Vaia, *Nat. Mater.*, **3**, 115 (2004).
11. M. Nie, D. M. Kalyon, and F. T. Fisher, *ACS Appl. Mater. Interfaces*, **6**, 14886 (2014).
12. M. Jonoobi, J. Harun, A. P. Mathew, and K. Oksman, *Compos. Sci. Technol.*, **70**, 1742 (2010).
13. Q. Kuang, D. Zhang, J. C. Yu, Y.-W. Chang, M. Yue, Y. Hou, and M. Yang, *J. Phys. Chem. C*, **119**, 27467 (2015).
14. E. Yilgor, T. Eynur, C. Kosak, S. Bilgin, I. Yilgor, O. Malay, Y. Menceloglu, and G. L. Wilkes, *Polymer*, **52**, 4189 (2011).
15. L. J. Bonderer, A. R. Studart, and L. J. Gauckler, *Science*, **319**, 1069 (2008).
16. A. F. Demirörs, D. Courty, R. Libanori, and A. R. Studart, *Proc. Natl. Acad. Sci. USA*, **113**, 4623 (2016).
17. R. M. Erb, R. Libanori, N. Rothfuchs, and A. R. Studart, *Science*, **335**, 199 (2012).
18. A. Noshay and J. E. McGrath, *Block Copolymers: Overview and Critical Survey*, Elsevier Science (2013).
19. P. Król, *Prog. Mater. Sci.*, **52**, 915 (2007).
20. M. Szycher, *Szycher's Handbook of Polyurethanes*, 1st Edition, Taylor & Francis (1999).
21. I. Yilgör, E. Yilgör, and G. L. Wilkes, *Polymer*, **58**, A1 (2015).
22. L. Bistričić, G. Baranović, M. Leskovac, and E. G. Bajsić, *Eur. Polym. J.*, **46**, 1975 (2010).
23. D. Cai, J. Jin, K. Yusoh, R. Rafiq, and M. Song, *Compos. Sci. Technol.*, **72**, 702 (2012).
24. B. Finnigan, K. Jack, K. Campbell, P. Halley, R. Truss, P. Casey, D. Cookson, S. King, and D. Martin, *Macromolecules*, **38**, 7386 (2005).
25. N. M. Girouard, S. Xu, G. T. Schueneman, M. L. Shofner, and J. C. Meredith, *ACS Appl. Mater. Interfaces*, **8**, 1458 (2016).
26. L. Jiang, C. Zhang, M. Liu, Z. Yang, W. W. Tjiu, and T. Liu, *Compos. Sci. Technol.*, **91**, 98 (2014).
27. D.-H. Kim, K.-C. Yu, Y. Kim, and J.-W. Kim, *ACS Appl. Mater. Interfaces*, **7**, 15214 (2015).
28. H. Kim, Y. Miura, and C. W. Macosko, *Chem. Mater.*, **22**, 3441 (2010).
29. S. M. Lai, C. K. Wang, and H. F. Shen, *J. Appl. Polym. Sci.*, **97**, 1316 (2005).
30. Y. Li, H. Chen, D. Liu, W. Wang, Y. Liu, and S. Zhou, *ACS Appl. Mater. Interfaces*, **7**, 12988 (2015).
31. R. Libanori, F. H. L. Münch, D. M. Montenegro, and A. R. Studart, *Compos. Sci. Technol.*, **72**, 435 (2012).
32. H. Liu, J. Song, S. Shang, Z. Song, and D. Wang, *ACS Appl. Mater. Interfaces*, **4**, 2413 (2012).
33. J. Pavličević, M. Špírková, M. Jovičić, O. Bera, R. Poręba, and J. Budinski-Simendić, *Composites Part B*, **45**, 232 (2013).
34. A. Pei, J.-M. Malho, J. Ruokolainen, Q. Zhou, and L. A. Berglund, *Macromolecules*, **44**, 4422 (2011).
35. Z. S. Petrović, I. Javni, A. Waddon, and G. Bánhegyi, *J. Appl. Polym. Sci.*, **76**, 133 (2000).
36. S. L. Phua, L. Yang, C. L. Toh, S. Huang, Z. Tsakadze, S. K. Lau, Y.-W. Mai, and X. Lu, *ACS Appl. Mater. Interfaces*, **4**, 4571 (2012).
37. L. Rueda, A. Saralegui, B. Fernández d'Arlas, Q. Zhou, L. A. Berglund, M. A. Corcuera, I. Mondragon, and A. Eceiza, *Carbohydr. Polym.*, **92**, 751 (2013).
38. M. Sadeghi, M. A. Semsarzadeh, M. Barikani, and M. Pourafshari Chenar, *J. Membr. Sci.*, **376**, 188 (2011).
39. N. Stribeck, A. Zeinolebadi, F. Harpen, G. Luinstra, B. Eling, and S. Botta, *Macromolecules*, **46**, 4041 (2013).

 DOI 10.1002/pen

40. Y. Xia, and R. C. Larock, *Macromol. Rapid Commun.*, **32**, 1331 (2011).
41. N. Yousefi, M. M. Gudarzi, Q. Zheng, X. Lin, X. Shen, J. Jia, F. Sharif, and J.-K. Kim, *Composites Part A*, **49**, 42 (2013).
42. I. S. Gunes, F. Cao, and S. C. Jana, *Polymer*, **49**, 2223 (2008).
43. I. S. Gunes and S. C. Jana, *J. Nanosci. Nanotechnol.*, **8**, 1616 (2008).
44. A. Pattanayak and S. C. Jana, *Polym. Eng. Sci.*, **45**, 1532 (2005).
45. C. Dubois, M. Rajabian, and D. Rodrigue, *Polym. Eng. Sci.*, **46**, 360 (2006).
46. S. M. Lai and S. D. Liu, *Polym. Eng. Sci.*, **47**, 77 (2007).
47. L. M. Chiacchiarelli, L. Monsalve, A. Vázquez, J. M. Kenny, and L. Torre, *Polym. Eng. Sci.*, **54**, 1817 (2014).
48. T. Hosseini-Sianaki, H. Nazockdast, B. Salehnia, and E. Nazockdast, *Polym. Eng. Sci.*, **55**, 2163 (2015).
49. E. Fortunati, F. Luzi, A. Janke, L. Häußler, J. Pionteck, J. M. Kenny, and L. Torre, *Polym. Eng. Sci.*, **57**, 521 (2017).
50. J. Xiong, Z. Zheng, X. Qin, M. Li, H. Li, and X. Wang, *Carbon*, **44**, 2701 (2006).
51. X. Cao, H. Dong, and C. M. Li, *Biomacromolecules*, **8**, 899 (2007).
52. G. Chen, S. Zhou, G. Gu, H. Yang, and L. Wu, *J. Colloid Interface Sci.*, **281**, 339 (2005).
53. Z. S. Petrović, Y. J. Cho, I. Javni, S. Magonov, N. Yerina, D. W. Schaefer, J. Ilavský, and A. Waddon, *Polymer*, **45**, 4285 (2004).
54. O. Malay, O. Oguz, C. Kosak, E. Yilgor, I. Yilgor, and Y. Z. Menceloglu, *Polymer*, **54**, 5310 (2013).
55. B. Wunderlich, *Thermal Analysis of Polymeric Materials*, Springer, Berlin Heidelberg, (2005).
56. I. Yilgor, E. Yilgor, I. G. Guler, T. C. Ward, and G. L. Wilkes, *Polymer*, **47**, 4105 (2006).
57. A. Beganskienė, V. Sirutkaitis, M. Kurtinaitienė, R. Juškėnas, and A. Kareiva, *Mater. Sci.*, (Medžiagotyra), **10**, 287 (2004).
58. F. E. Bailey and J. V. Koleske, *Poly(ethylene oxide)*, Academic Press (1976).
59. T. D. Fornes and D. R. Paul, *Polymer*, **44**, 4993 (2003).
60. D. Gersappe, *Phys. Rev. Lett.*, **89**, 058301 (2002).
61. D. Shah, P. Maiti, D. D. Jiang, C. A. Batt, and E. P. Giannelis, *Adv. Mater.*, **17**, 525 (2005).
62. T. H. Zhou, W. H. Ruan, M. Z. Rong, M. Q. Zhang, and Y. L. Mai, *Adv. Mater.*, **19**, 2667 (2007).